Supplement of Atmos. Chem. Phys., 26, 11943–11965, 2026
https://doi.org/10.5194/acp-26-11943-2026-supplement

Atmospheric Chemistry and Physics
Open Access
EGU

Supplement of

Precursor dynamical factors in the local lower atmosphere of warm-sector heavy rainfall over South China: evidence from wind profiler radar observations

Wanju Li et al.

Correspondence to: Yuanjian Yang (yyi1985@nuist.edu.cn)

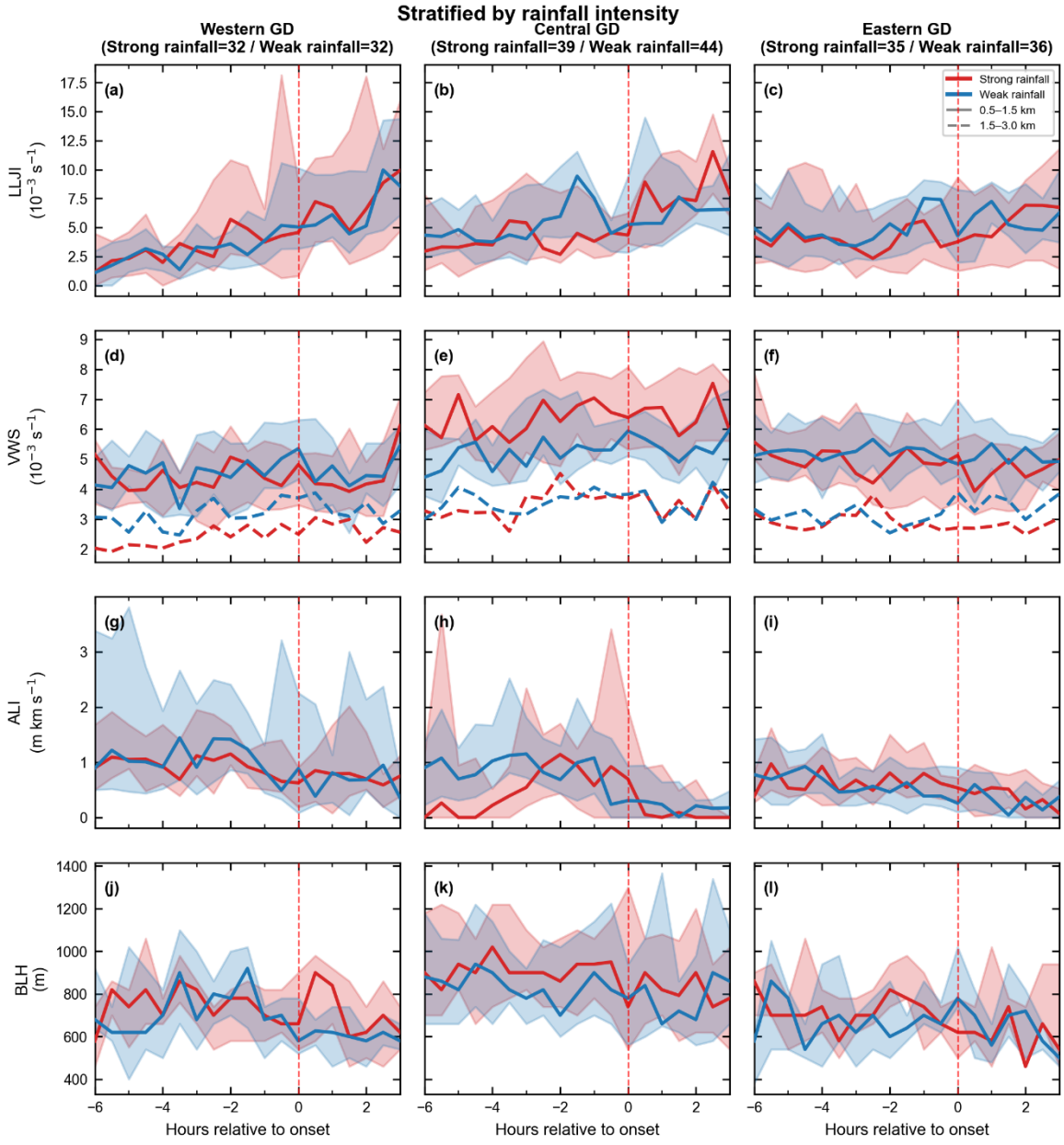

Figure S1. Stratified composite time series of precursor indices (LLJI, VWS, ALI, and BLH) for WSHR events across three sub-regions, categorized by rainfall intensity.

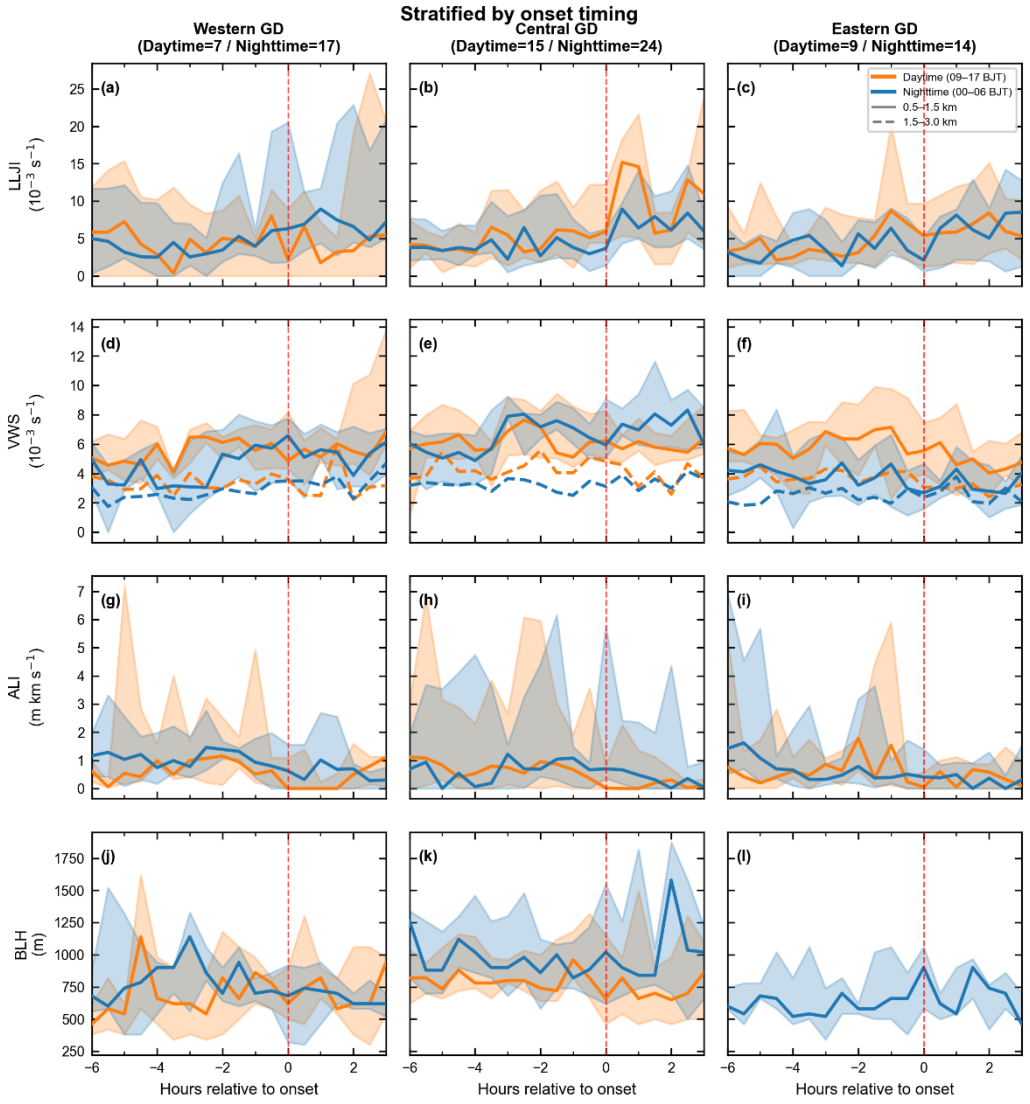

Figure S2. Stratified composite time series of precursor indices (LLJI, VWS, ALI, and BLH) for WSHR events across three sub-regions, categorized by onset timing (Daytime vs. Nighttime).

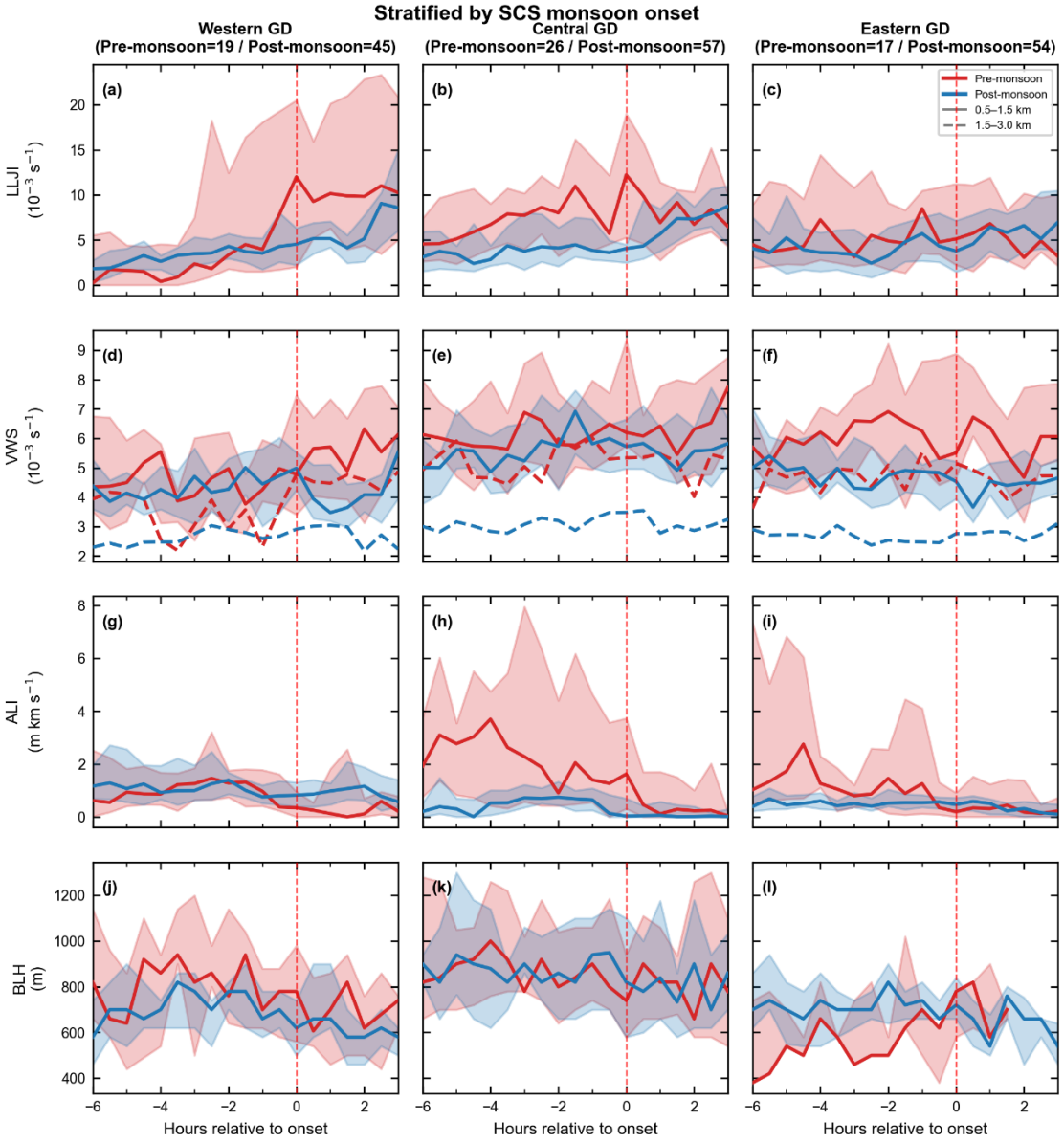

Figure S3. Stratified composite time series of precursor indices (LLJI, VWS, ALI, and BLH) for WSHR events across three sub-regions, categorized by the South China Sea (SCS) monsoon onset (Pre-monsoon vs. Post-monsoon).

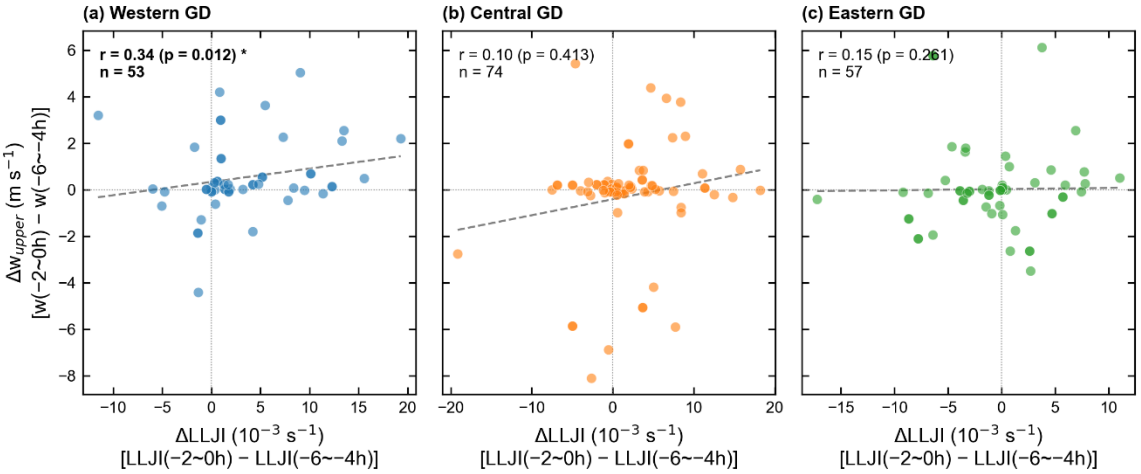

Figure S4. Spearman rank correlations between the pre-onset change in the LLJI (**Δ*LLJI***) and the upper-level (3–5 km) vertical velocity change (**Δ*w***) for (a) western GD, (b) central GD, and (c) eastern GD.

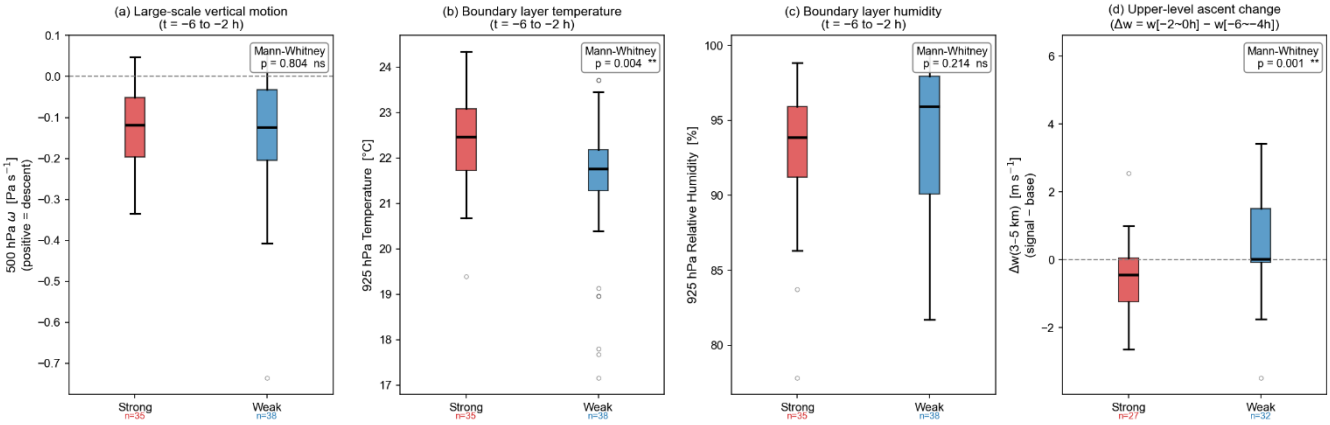

Figure S5. ERA5-derived pre-onset diagnostics (t = −6 to −2 h) for strong-rainfall (red) and weak-rainfall (blue) events in eastern GD. (a) 500 hPa vertical velocity (positive = descent). (b) 925 hPa temperature. (c) 925 hPa relative humidity. (d) Upper-level vertical velocity change (Δw at 3–5 km; definition as in Fig. 12). Box plots show the median, interquartile range, and 1.5 × IQR whiskers. Mann-Whitney p values and significance levels are annotated.

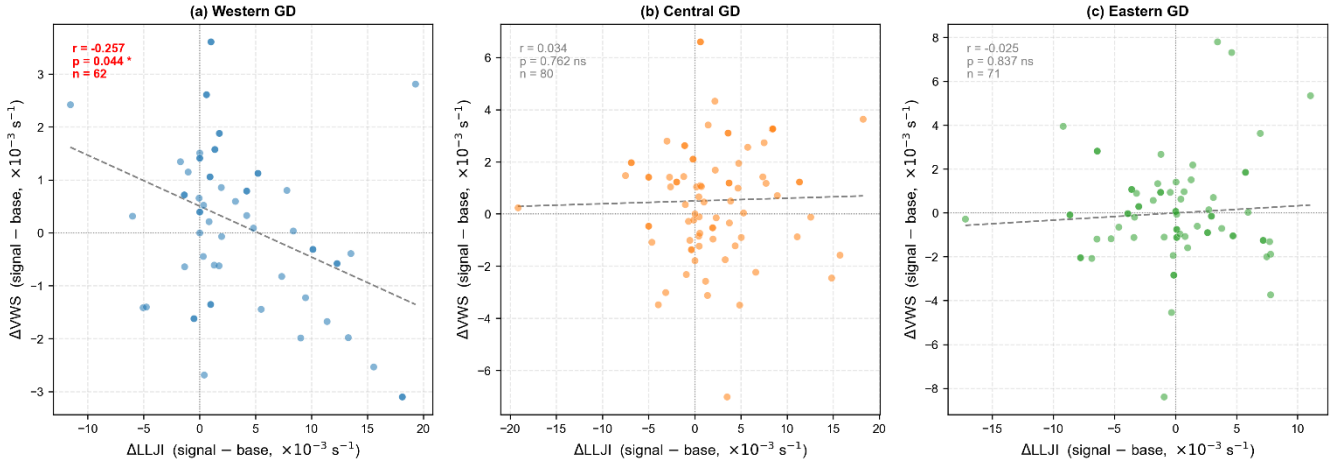

Figure S6. Scatter plots of ΔLLJI versus ΔVWS for (a) western GD, (b) central GD, and (c) eastern GD. Δ denotes the difference between the signal period (t = −2 to 0 h) and the baseline period (t = −6 to −4 h). Dashed lines show linear fits. Spearman r, p value, and sample size are annotated; red text indicates p < 0.05.

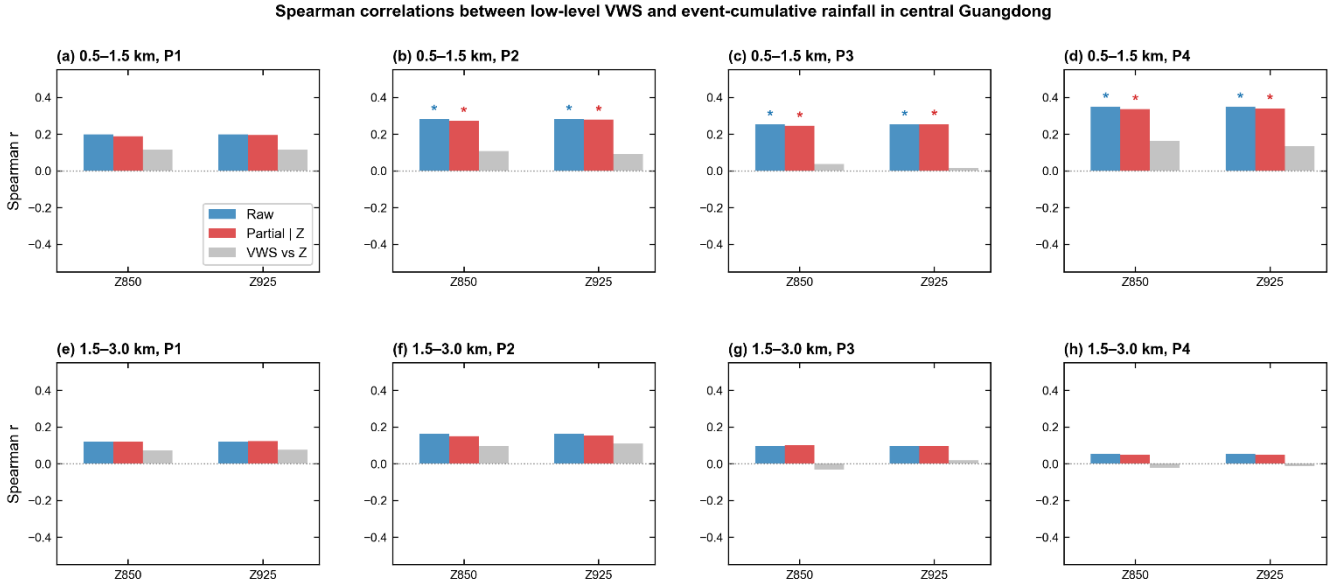

Figure S7. Spearman partial correlations between low-level VWS and event-cumulative rainfall across the 88 events, controlling for concurrent ERA5 geopotential height over central GD. Results are shown for two VWS layers (0.5–1.5 km, primary; 1.5–3.0 km, control) and four pre-onset windows (P1: −6 to −4 h; P2: −4 to −2 h; P3: −2 to −1 h; P4: −1 to 0 h), with Z_{850} and Z_{925} as control variables. Blue bars show raw Spearman correlations; red bars show partial correlations after controlling for Z; grey bars show the auxiliary Spearman correlation between VWS and Z itself. Asterisks mark p < 0.05 (*).

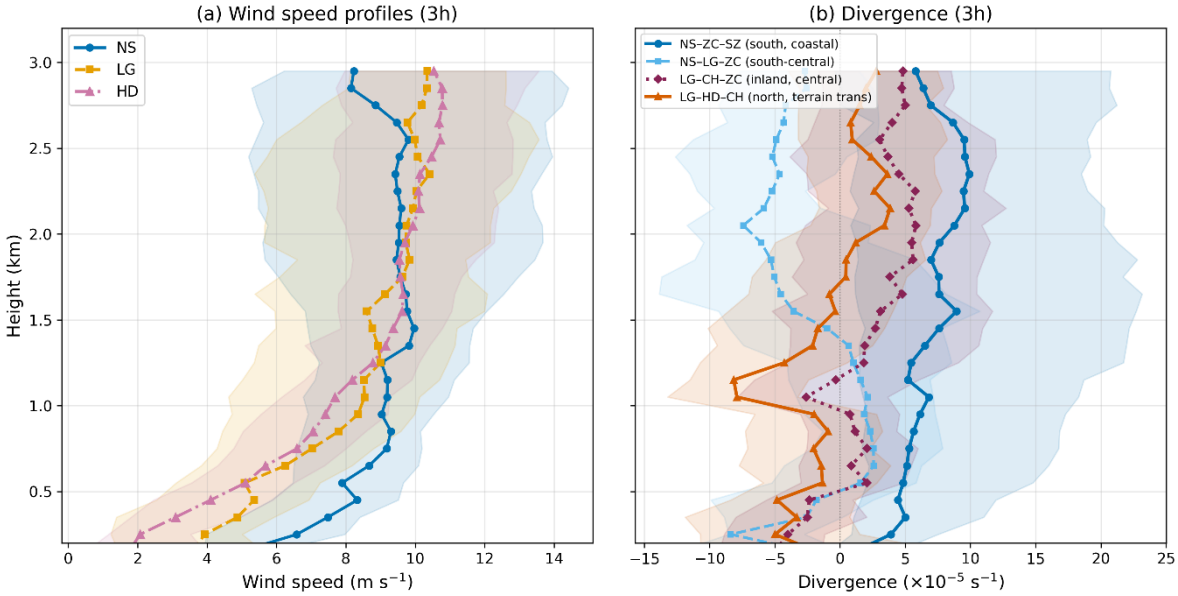

Figure S8. As Fig. 17, but showing event composite absolute fields rather than anomalies. (a) Event wind speed profiles at NS, LG, and HD. (b) Event divergence profiles for the four Bellamy triangles. Shading denotes interquartile ranges.

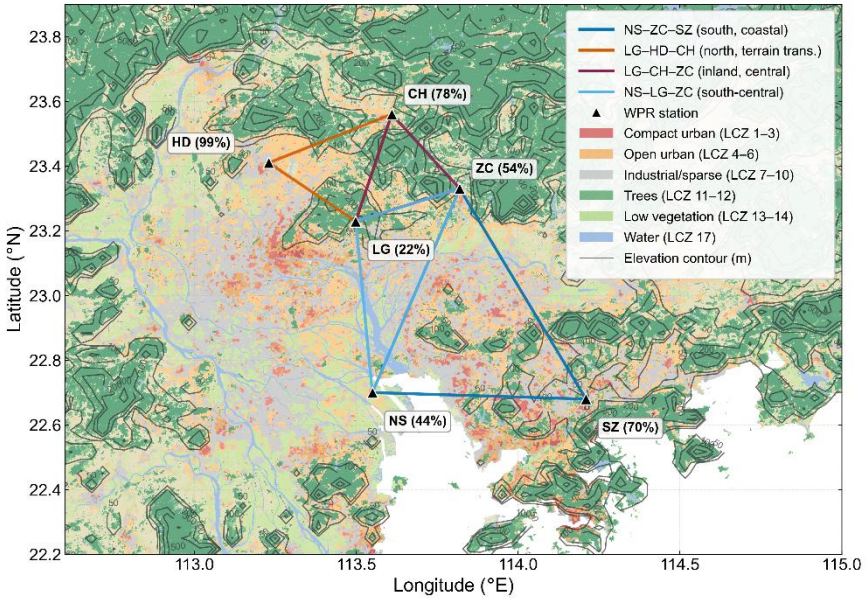

Figure S9. Geographic distribution of the six wind profiler stations used in the triangle divergence analysis (black triangles) and the four Bellamy triangles overlaid on the local climate zone (LCZ) classification. LCZ categories are grouped as: compact urban (LCZ 1–3, red), open urban (LCZ 4–6, orange), industrial or sparsely built (LCZ 7–10, grey), trees (LCZ 11–12, dark green), low vegetation (LCZ 13–14, light green), and water (LCZ 17, blue). Grey contours show terrain elevation (50, 100, 200, 300, 500, 800 m). Station labels include the 3-km urban fraction in parentheses. Triangle colours match those in Fig. 17b.